

Path Performance Optimization of Complex Flight Mechanics Models Using Reduced-Order Modeling

Johanes, Reggie; Oliviero, Fabrizio; Varriale, Carmine

DOI

10.13009/EUCASS2025-097

Publication date

Document Version Final published version

Citation (APA)

Johanes, R., Oliviero, F., & Varriale, C. (2025). Path Performance Optimization of Complex Flight Mechanics Models Using Reduced-Order Modeling. Paper presented at 11th European Conference for AeroSpace Sciences (EUCASS), Rome, Italy. https://doi.org/10.13009/EUCASS2025-097

To cite this publication, please use the final published version (if applicable). Please check the document version above.

Copyright

Other than for strictly personal use, it is not permitted to download, forward or distribute the text or part of it, without the consent of the author(s) and/or copyright holder(s), unless the work is under an open content license such as Creative Commons.

Please contact us and provide details if you believe this document breaches copyrights. We will remove access to the work immediately and investigate your claim.

Path Performance Optimization of Complex Flight Mechanics Models Using Reduced-Order Modeling

Reggie Johanes, Fabrizio Oliviero, and Carmine Varriale[†]
Delft University of Technology
Delft, The Netherlands
F.Oliviero@tudelft.nl · C.Varriale@tudelft.nl
[†]Corresponding author

Abstract

Path performance optimization has proven to be a powerful tool in solving a wide variety of optimal control problems in the aerospace field. However, the numerical complexity of such methodologies often prevents the possibility to optimize the performance of high-fidelity flight mechanics models characterized by coupled, non-linear, and/or high-order dynamic and aero-propulsive models. This research has explored the impact of reduced-order modeling on the optimal path performance obtainable with surrogates of the high-fidelity flight mechanics model. The developed methodology revolves around the creation of different reduced-order models that retain the characteristics of a full-order flight mechanics model to different degrees of fidelity, while being manageable by an optimal control solver. The methodology has been applied to obtain minimum-time landing trajectories for the UNIFIER19 C7A, a hybrid-electric aircraft featuring over-the-wing distributed propulsion, previously developed under the UNIFIER19 project. Results show that the reduced-order models can be used to generate flyable trajectories, as verified by tracking the resulting landing approach paths using the base high-fidelity model. On the other hand, the value of the objective function differs widely depending on the reduced-order model used, indicating that the modeling choice has a significant impact on the optimal performance prediction.

Symbols and Abbreviations

α	Angle of attack
C_L	Total lift coefficient
C_D	Total drag coefficient
C_M	Pitching moment coefficient
D	Drag force
δ	Control surface deflection

 δ Control surface deflection g Gravitational acceleration

L Lift force mass

M Pitching moment

q Pitch rate t Time θ Pitch angle

u Horizontal velocity, body axis

w Vertical velocity, body axis

x Horizontal pos., NED ref. framez Vertical pos., NED ref. frame

h Altitude, positive up V_a True airspeed

CFD Computational Fluid Dynamics DEP Distributed Electric Propulsion

DoF Degree of Freedom
HFM High-Fidelity Model
HTU Horizontal Thrust Unit
LSED Lock-Step Euclidean Distance

ROM Reduced-Order Model

1. Introduction

A path performance optimization problem aims to find the best performance for a dynamic system, according to a certain metric, over a certain period of time and while subject to a set of constraints.¹ Practical applications of path performance optimization have been developed for a variety of fields, such as robotics,² spacecraft,³ aircraft,⁴ and marine navigation.⁵ In aviation, path performance optimization has been widely utilized in the effort to minimize the environmental impacts associated with aircraft operations.⁶ Prime examples include studies on the minimization of fuel consumption, greenhouse gas emissions, and noise impact throughout all flight phases. As the aviation industry

continues to innovate towards the future of green aviation,⁷ path performance optimization remains an indispensable tool to meet ambitious climate goals.

Despite its proven utility, one constraining aspect of trajectory optimization is the difficulty in performing such an analysis with a high-fidelity flight mechanics model, characterized by coupled, non-linear, and high-order dynamics.^{4,8} This issue is exacerbated when novel technologies and configurations, such as a hybrid powertrain or a distributed propulsion system, require more degrees of freedom to fully describe their dynamic behavior. In these cases, transcribing the equations of motion to solve the trajectory optimization problem becomes intractable, and some studies have been conducted with lower-order models (such as point mass models)^{9,10} to compromise between physical accuracy and computational feasibility.

This research implements a path performance optimization problem using different Reduced-Order Models (ROMs) to represent the aero-propulsive characteristics of a hybrid electric aircraft utilizing 12 propulsors along the wingspan as a Distributed Electric Propulsion (DEP) system. The aircraft model under observation is the final configuration proposed by the EU-funded UNIFIER19 project, ¹¹ for which High Fidelity Models (HFM) for the aero-propulsive characteristics were produced by an extensive Computational Fluid Dynamics (CFD) analysis, and a simulation of all the powertrain elements were included in a 6 Degrees of Freedom (DoF) simulator of the aircraft.

Multiple methods have been developed and implemented to construct such ROMs. ^{12–15} A popular example among many is the use of neural networks to represent complex nonlinear systems. In the context of flight dynamics modeling, neural networks can be used to approximate aerodynamic coefficients, effectively replacing cumbersome lookup tables that contain data obtained from CFD analysis or wind tunnel testing. By doing so, memory requirements are reduced while allowing differentiable approximations to be used and nonlinearities to be modeled. For this study, however, a simpler concept of reduced-order modeling is employed to allow the methodology to be easily applied to any existing HFM.

In this study, the original (base) model is reduced in two ways. First, the aerodynamic model of the aircraft is simplified by reducing the distributed aero-propulsive forces into a single point. Second, the 6 DoF flight dynamics model is replaced with a 3 DoF representation of the system.

The use of lookup tables is preserved to maintain the correct dependencies of the aero-propulsive forces with respect to the flight parameters. Different ROMs are created by making choices on the number of aerodynamic dependencies to be accounted for. For instance, the overall lift coefficient of the aircraft may be a function of a number of parameters such as its angle of attack, flap deflection, DEP advance ratio, and elevator deflection. However, one or more of these dependencies may be left out to simplify the aerodynamic model and reduce computational costs. The effect that these omissions have on the accuracy of the reduced order model and on the optimal performance prediction will be the object of investigation.

To confirm that the ROM maintains a sufficient degree of physical accuracy with respect to the HFM, the optimal trajectories will be tracked by the high-fidelity model. The *trackability* of the optimal trajectory will then serve as a representation of the so-called reconstruction error of the reduced-order modeling process.

2. Models

2.1 Reference Aircraft

The subject of this study is the UNIFIER19 C7A aircraft, a hybrid electric fixed-wing aircraft designed to carry nineteen passengers for commuter operations.¹¹ Its propulsion system comprises twelve distributed electric propulsors and one Horizontal Thrust Unit (HTU) propulsor mounted on the aft of the fuselage. It has a high-mounted, unswept main wing and a v-tail empennage configuration that houses its six control surfaces. These control surfaces are the right and left ailerons and flaps on the main wing, as well as the pair of ruddervators for pitch and yaw control on the empennage. Figure 1 illustrates the layout of all effectors on the UNIFIER19 C7A and its top-level specifications are presented in Table 1.

By positioning the twelve propulsors along the entire span of the main wing, the blown-wing effect is utilized to increase the aircraft's lift coefficient. Combined with the use of trailing edge flaps, this allows the aircraft to produce an increased amount of lift at relatively low airspeeds, enhancing the aircraft's short-field performance. Additionally, the tail-mounted HTU can also act as a drag generator by producing negative thrust at certain conditions. This allows the aircraft to maintain flight at even lower airspeeds, as the DEP is activated to increase lift while the HTU produces additional drag to offset the horizontal acceleration produced by the high DEP setting. At cruise, the use of the DEP is inefficient. Therefore, the DEP propellers are designed to be folded when not in take-off/landing conditions, while the HTU alone provides the necessary thrust.

The design of the UNIFIER19 C7A aircraft, including the methods used in the design process, is thoroughly documented in the project's design report. 11 As part of the project, a Simulink-based flight dynamics simulator was also

Table 1: UNIFIER19 top-level aircraft s	specifications ¹¹
---	------------------------------

Variable	Value	Unit
MTOW	7954	kg
Passenger Capacity	19	-
Wingspan	20.11	m
Cruise Range	350	km
Cruise Altitude	1219	m
Cruise Speed	72.7	m/s

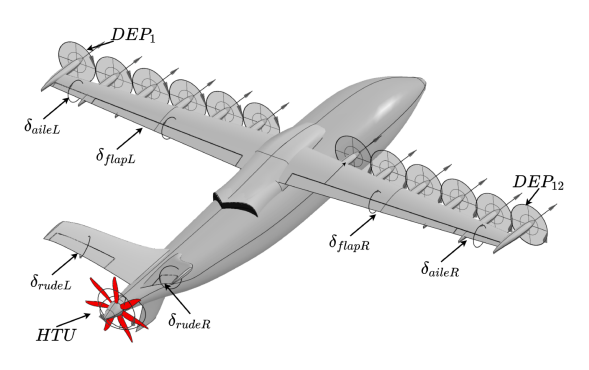


Figure 1: UNIFIER19 C7A effectors.¹⁷

constructed. The simulator is complemented with detailed aerodynamic and propulsive models, which are described in detail in the simulator documentation. ¹⁶

2.1.1 Aero-Propulsive Model

The core of the UNIFIER19 C7A flight dynamics simulator is its aerodynamics and propulsive models.

Aerodynamic data was calculated, by means of the Flightstream panel-method solver, for the isolated elements of the aircraft, namely the empennage, fuselage, and main wing. As a result, multidimensional lookup tables collected from the analysis can be used to evaluate the forces generated by each element and, consequently, the total forces and moments acting on the aircraft's center of gravity are then derived as a summation of the various contributions. By doing so, inter-component interactions, such as the effect of having the main wing blown by the DEP, can be more accurately accounted for. This capability is especially important for the UNIFIER19 C7A aircraft, given the high coupling between aerodynamic surfaces and propulsion elements. If these dependencies were to be captured by a full-model analysis without component splitting, vastly more computational resources would be needed.

The propulsive model comprises the DEP and HTU systems. For the DEP system, an electric motor model and propeller model are used to represent each propulsor. A unit-less value termed the *activity factor* is used as the input to the model. The value of the activity factor ranges from 0 to 1, corresponding to a thrust request of zero and maximum thrust, respectively. A lookup table is then used to evaluate the RPM needed to achieve the desired thrust level. As the propeller operates at a fixed pitch, only one RPM will generate a specific thrust for a given airspeed. The RPM command is then fed to the electric motor model, which produces the actual RPM. Subsequently, the propeller model calculates the torque and thrust on the basis of the motor's RPM. The advance ratio is also calculated as an input to the aerodynamic model. This allows for the aero-propulsive interactions over the main wing to be accounted for.

The HTU is modeled similarly to the DEP with two key differences. First, the activity factor for the HTU may have a negative value to represent the use of the propeller as a drag generator. Second, the HTU employs a variable pitch propeller. Consequently, calculating the optimal RPM from the activity factor is more complex than the DEP model. To solve this, XROTOR was used to generate a 4D lookup table for the HTU in the HFM. The lookup table contains HTU torque as a function of RPM, airspeed, and thrust. The torque lookup table is subsequently used to construct the power lookup table, with which the optimum RPM can be evaluated at a given airspeed and desired thrust.

As the aerodynamic and propulsive models were constructed on a component level, a complex interpolation procedure is needed to compose the total forces and moments acting on the aircraft as a whole. In summary, this procedure involves calculating local angles of attack, sideslip, and flow velocities at numerous stations on the main wing and empennage before utilizing the collected lookup tables to produce the forces and moments at each segment. Lastly, interactions between the main wing and tail as well as the aerodynamic contributions from non-lifting components are also accounted for when summing the forces and moments.

2.2 Flight Dynamics Model

While the reference model from the UNIFIER19 project allows for a full 6 DoF simulation, this study is limited to longitudinal flight only. Therefore, a 3 DoF flight dynamics model is used to simulate translational motion in the x and z Earth axes, together with aircraft pitch rotation in the longitudinal plane. Other classic assumptions are also adopted. Namely: (a) the aircraft is assumed to be a rigid body; (b) the Earth is assumed flat and non-rotating; (c)

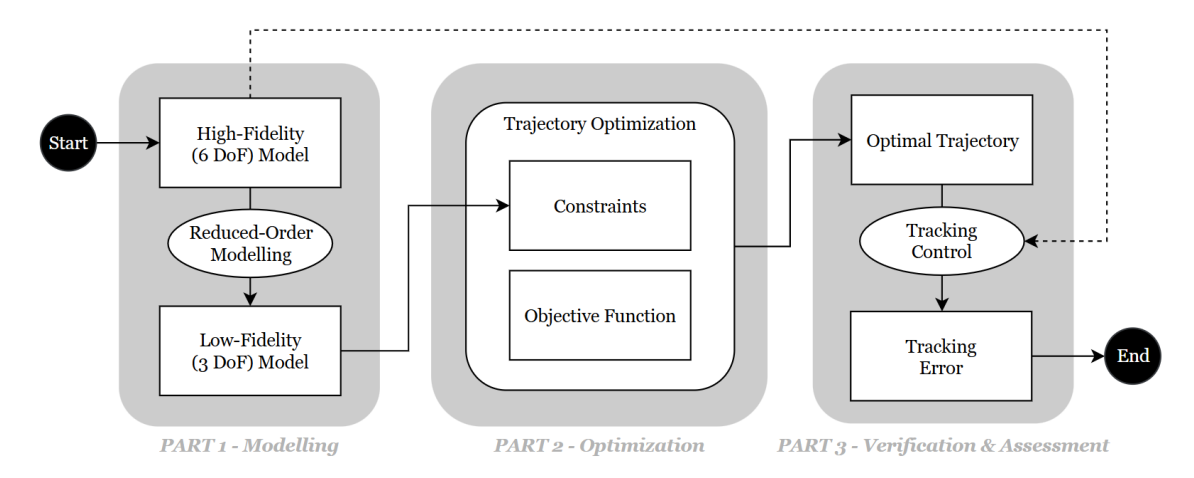


Figure 2: Research methodology

gravity is constant; (d) undisturbed still air is assumed; (e) aircraft weight and inertia are constant; (f) the aircraft has a longitudinal symmetry plane; (g) International Standard Atmosphere (ISA) is considered.

In this contest, the aircraft dynamic model consists of 6 states X: positions along the horizontal and vertical axes of the flat Earth reference frame x and z, horizontal and vertical velocities relative to the body reference frame u and w, pitch angle and pitch rate θ and q. It also has 4 control variables U: the elevator and flap deflections δ_{elev} and δ_{flap} , and the DEP and HTU activity factors.

$$X = \{x, z, u, w, \theta, q\} \qquad U = \{\delta_{\text{elev}}, \delta_{\text{flap}}, \text{DEP}, \text{HTU}\}$$
 (1)

It is explicitly noted that the DEP system could in principle provide also additional authority and control in yaw by exploiting differential thrust. In fact, in the reference model, this is accounted by means of a butterfly shaped linear distribution of thrust, depending on the spanwise location of each propulsor. Given the scope of the present study, focused solely on the longitudinal trajectory, this capability is not considered.

Implementation of the equations of motion for this model utilized MATLAB Simulink's 3D0F (Body Axes) block from the Aerospace Blockset.¹⁸ The classic equations of motion for a 3-DoF flight mechanics model have been used, and are not reiterated here.

3. Methodology

As shown in Figure 2, the research activities carried out within this thesis project are broadly grouped into three major parts: modeling, optimization, and verification. The first part focused on deriving the aircraft ROM from its HFM. This is done by simulating the base HFM and utilizing the extracted data to construct lookup tables for the ROMs. In addition, depending on the scope of the analysis, a trimming condition is enforced to guarantee the equilibrium of the system during the whole trajectory.

The resulting ROMs are then implemented as dynamics constraints in the path performance optimization problem. The optimization problem is formulated in the second part. The feasibility of the resulting trajectory is then verified in the last part, where it is tracked by the HFM using feedback control. Several versions of the ROM have been constructed with varying degrees of fidelity. The entire process, represented in Figure 2, has been repeated for each variation.

3.1 Reduced-Order Modeling

The base HFM described in Section 2.1.1 was simplified by reducing only the aerodynamic model, while the propulsive model was used as is. This approach was chosen in light of the relative complexity of the aerodynamic model. While the latter is structured as a summation of many components, the propulsive model only requires calculations for twelve (identical) DEP propulsors and one HTU. Moreover, as the HFM already directly converts the advance ratio to the thrust coefficient using a lookup table, it is not possible to further simplify the DEP model without losing the ability to account for aero-propulsive interactions and the blown-wing effect.

To build the reduced aerodynamic model, three lookup tables were used to evaluate the lift, drag, and pitching moment coefficients. These lookup tables were constructed by simulating the HFM at varying flight conditions

Variable	Description	Unit	Min	Max	Increment
α	Angle of attack	deg	-40	40	1
$\delta_{ m elev}$	Elevator deflection	deg	-30	30	5
$\delta_{ m flap}$	Flap deflection	deg	0	25	5
DEP	DEP activity factor	_	0	1	0.1

Table 2: Input variables for generation of the ROMs

and recording the instantaneous total aerodynamic forces and moment at each condition. The respective coefficients themselves were then obtained by non-dimensionalizing the forces and moments in the usual way. The execution of this procedure can be intuitively understood as conducting a "virtual wind tunnel" experiment, where the aircraft was placed at varying angles of attack, with different combinations of control surface deflections and thrust configurations, while the resulting forces were recorded. The conditions and inputs that were varied for this evaluation, along with their ranges and increments are shown in Table 2.

While the DEP activity factor is used as an input to the ROM evaluation procedure, the advance ratio J will be used in its place as an input to the resulting lookup tables. The advance ratio produced at each DEP setting is therefore calculated and stored to be used as breakpoints in the resulting lookup tables, along with the original ranges of α , δ_{elev} , and δ_{flap} . This was done to better represent the aero-propulsive interactions as they are physically linked to the advance ratio, as opposed to simply the DEP setting. A limitation of this method is that the range of advance ratios produced, and therefore the range of advance ratios at which the ROM is able to evaluate the aerodynamic coefficients, is determined by the (fixed) airspeed at which the ROM is evaluated. Therefore, an airspeed values of 50 m/s has been considered as a sufficient compromise to cover the range of advance ratios for the landing simulated in this study.

To further investigate the trade-off between accuracy and computational efficiency, multiple versions of the ROM are constructed with varying numbers of dependencies accounted for. The resulting reconstruction error obtained with these models is then compared to gain insights into the optimal level of fidelity needed to achieve satisfactory accuracy while minimizing computational costs and allowing convergence during trajectory optimization.

The variations in dependencies will be produced by fixing the value of one or more of the independent parameters, effectively using only a subset from the complete collected dataset for a particular coefficient. Three ROM versions are generated with version 1 (v1) being the reduced base dataset retaining all dependencies, and version 3 (v3) is the simplest. A summary of the different ROM versions produced and the dependencies included for each coefficient is shown in Table 3, also showing the values at which some of the parameters are fixed for the simpler ROMs. For both v2 and v3, the advance ratio is fixed to a value that would correspond to a 0.5 DEP activity factor setting.

Dependencies Included **ROM** Coeff. Version δflar C_L v1 C_{D} См C_{L} C_D v21.67 См C_L Selev = (DEP =0 deg $\delta flap =$ v3 C_{D} 5 deg C_{M}

Table 3: Dependencies for each ROM version

3.2 Trimming

The initial conditions for the path performance optimization and the trackability simulation require the aircraft to be trimmed at steady, straight, and level flight. Therefore the trim states and controls need to be calculated for the HFM as well as all ROM versions. In order to do this, the trim problem is formulated as an unconstrained optimization problem. A subset of the states and controls introduced in Section 2.2 are used to constitute the trim decision vector. The objective function is formulated to minimize residual accelerations, which are calculated using each aircraft model.¹⁹

The trim problem is solved using MATLAB's fmincon,²⁰ using the interior point algorithm with the forward finite difference gradient calculation. The bounds for the decision variables are determined based on physical constraints and control surface saturation limits. Tolerances as well as the DiffMinChange setting were adjusted on a case-by-case basis depending on the target trim conditions and model used in order to improve convergence results.

3.3 Path Performance Optimization

Optimization of path performance is achieved in the framework of Optimal Control Theory, where the time-histories of the control and state variables are unknown, and they are to be varied by the optimizer to minimum with a certain objective function in the presence of bounds and constraints.

Classic direct resolutions methods require transcribing the infinite dimensional problem (in the continuous time domain) into a discrete one, so that optimization can be applied to a finite set of variables: the values of the controls at certain point in time. In the present study, the optimization was performed using the open-source ICLOCS2 (Imperial College London Optimal Control Software) suite,²¹ using a transcription method based on Hermite-Simpson collocation. The transcribed problem was then solved using IPOPT (Interior Point Optimizer)²² as the Nonlinear Programming solver. For its resolution, both initial and final conditions on the states need to be determined.

The initial condition refers to the start of landing phase, where the aircraft is in straight and level flight at an altitude of 1219 m with an airspeed of 72.7 m/s. It is assumed that the flaps are deployed at a 5 deg deflection angle, and their deployment is maintained constant during the whole phase. The HFM allows simulating the flight dynamics also for different values of the flap deflection, but this would have required much more complex multiphase path performance optimization, not interesting in the scope of this study.

The landing phase is considered complete when the aircraft reaches an altitude of $5 \, \text{m}$. Additionally, the initial guess for the terminal conditions utilizes the states and controls of the aircraft trimmed for steady level flight at $5 \, \text{m}$ altitude with an airspeed of $50 \, \text{m/s}$, after descending at an average glide slope of $1 \, \text{deg}$.

The optimization minimizes the total flight time t_f , as it is considered the simplest metric to evaluate the performance of the aircraft. This term is regarded as a Mayer cost term in the objective function. To incentivize utilization the DEP system in enhancing low speed performance, a Lagrange (stage cost term) term is also included in the objective function, to promote lower airspeeds (and hence higher lift coefficients) at low altitudes. The stage cost function consists of the product between the current airspeed and a penalty factor which increase exponentially as the altitude decreases. The complete objective function is shown in Equation 2.

$$\min_{X(t),U(t)} t_f + \int_{t_0}^{t_f} 0.1 \cdot \exp\left(\frac{z(t) - z_0}{z_0}\right) \cdot \frac{V_a(t)}{V_{a_0}} dt$$
 (2)

3.3.1 Bounds

Control variables bounds are simply the system saturation and rate limits as described by the HFM simulator documentation. Bounds used for the state variables are summarized by Table 4. The bounds for u and w were chosen such that any combination of the two variables could not result in airspeeds lower than the stall speed and/or angles of attack beyond the range of the ROM breakpoints.

Variable	Lower Bound	Upper Bound	Unit
X	0	+∞	m
z	$-\infty$	0	m
и	35 cos (20 deg)	75	m/s
w	75 sin (20 deg)	75 sin (20 deg)	m/s
θ	-5	5	deg
q	-2	2	deg/s

Table 4: Bounds for the state variables

3.3.2 Constraints

Multiple path and boundary constraints are also imposed on the problem in order to ensure a realistic solution. They are summarized in Table 5.

The rate of climb is limited to a minimum of $-350 \, \text{m/s}$ to promote ride quality by preventing excessively quick descents. It was also limited to a maximum of $0 \, \text{m/s}$ to prevent the aircraft from climbing at any point in the trajectory. The angle of attack range was chosen in order to stay within the linear part of the lift curve slope. The airspeed was limited by two constraints. First, an inequality constraint was imposed to limit the aircraft to fly between 110% of the stall speed and $80 \, \text{m/s}$. This was done to prevent the aircraft from flying too close to the stall speed and to prevent excessive increases in airspeed beyond the initial cruise speed. Lastly, a narrower airspeed range was applied on the final instant, where a maximum of 130% of the stall speed is imposed in order to obtain realistically slow approach speeds. The end boundary constraint, combined with the stage cost function described above, was implemented to promote the usage of the DEP, which is a key feature of the aircraft allowing for enhanced low-speed performance.

Type	Variable	Unit	Lower bound	Upper bound
	Rate of climb	ft/min	-350	0
Path	Angle of attack	deg	-15	10
	True airspeed	m/s	39.4	80
End boundary	True airspeed	m/s	39.4	46.6

Table 5: Constraints for the path performance optimization problem

3.4 Tracking

The final part of the study involves tracking the resulting optimal trajectory using the HFM. The trackability of the trajectory, expressing how closely the HFM can follow the optimal trajectory obtained with a ROM, will then be used as a measure of the reduced-order model's reconstruction error of the original model performance. To achieve this, PID controllers are used to construct a simple tracking control system. In order to track the two-dimensional reference trajectory, an airspeed and altitude controller are implemented in the MATLAB Simulink environment.

The altitude tracking system consists of a cascaded loop which controls the aircraft altitude by means of elevator commands, and is represented in Figure 3. The outermost loop receives the current altitude as feedback and compares it to the reference altitude. A Proportional-Integral (PI) controller then receives the altitude error and produces a target pitch angle for the inner loops. The two inner loops constitute the pitch attitude control system. Pitch angle feedback also provides an effective method to stabilize the phugoid mode of the aircraft. Therefore, the pitch attitude control system also acts as a phugoid damper. Both inner loops were tuned using Simulink's PID Tuner App, while the outermost loop was tuned manually by trial and error, as the step response from the PID Tuner App for the outer loop produced an excessively slow settling time.

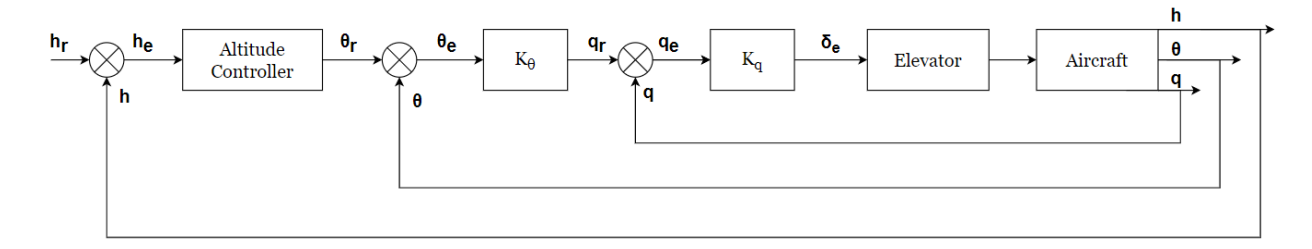


Figure 3: Altitude control system

The airspeed controller consists of a single loop, as the airspeed typically has a slow response, and is shown in Figure 4. A single PI controller is used to eliminate steady-state error.²³ The controller receives the airspeed error and computes the appropriate throttle input, which is then fed to the aircraft model. A limitation of this control system is that the same commands are given to both the DEP and HTU. This means that it is not possible for the controller to fully utilize the DEP activity factor while using the HTU in regenerative mode. The airspeed controller was also tuned manually, for similar reasons as the altitude controller above.

To quantify how closely the trajectory of a ROM is tracked by the HFM, the average Lock-Step Euclidean Distance (LSED) similarity measurement has been used (Equation 3). This measures the average Euclidean distance

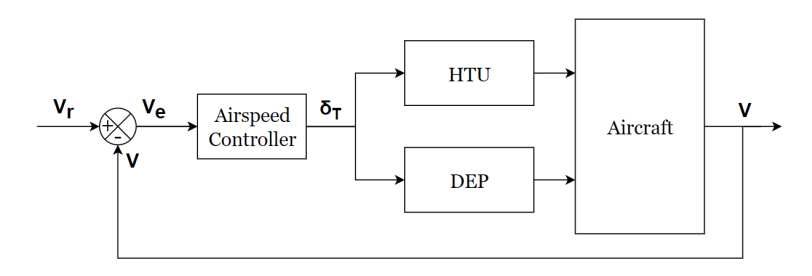


Figure 4: Airspeed control system

between the reference trajectory and the tracking one over the entire evolution.²⁴

LSED_{avg} =
$$\frac{1}{n} \sum_{i=1}^{n} \sqrt{(x_{\text{ref}_i} - x_{\text{track}_i})^2 + (z_{\text{ref}_i} - z_{\text{track}_i})^2}$$
 (3)

The LSED has a relatively straightforward physical interpretation, and works well when the reference and tracking trajectories have the same number of time steps. Whereas both the altitude and airspeed are used as top-level controller references, only the error in the geometric position of the aircraft is considered.

4. Results and Discussion

4.1 Reduced-Order Modeling

Figure 5 shows a sample of the resulting lift, drag, and pitching moment coefficient curves obtained with the ROM procedure outlined in section 3.1. It can be seen that the HFM only produces accurate aerodynamic data between angles of attack of -15 to 20 degrees, and interpolation is used beyond those limits. This is consistent with the range used for aerodynamic data collection when the HFM was constructed. It is also observed that the lift coefficient curve is linear between the angles of attack of -15 to 10 degrees, which are used as constraints for the trajectory optimization procedure. An increase in flap deflection is seen to raise both the lift and drag coefficient curves without altering its overall profile, although the amount raised is not constant at every angle of attack. On the other hand, increasing flap deflection results in an increase in the steepness of the C_{M_0} slopes, meaning longitudinal stability is improved.

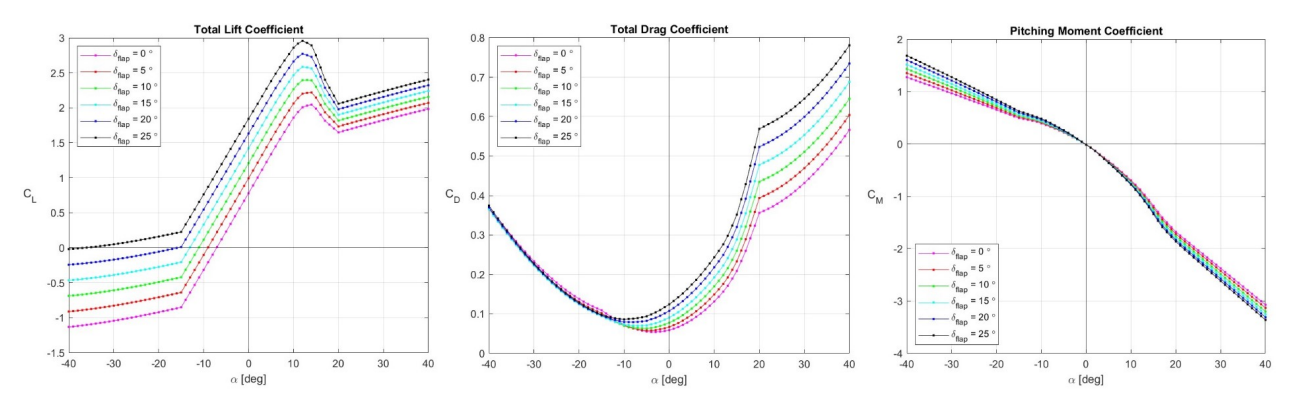


Figure 5: ROM lift, drag, and pitching moment coefficient curves at DEP = 0.5, δ_{elev} = 0 deg

Several comparisons have then been conducted to study the differences among the three ROM models, also with respect to the baseline HFM. First, each ROM has been trimmed to compare the different inputs required to achieve the same steady-level flight at terminal landing conditions. The results are shown in Table 6. ROMv1 and ROMv2 require a higher angle of attack compared to the HFM, while the opposite is true for ROMv3. The lack of the elevator deflection dependency on the lift and drag coefficients for ROMv3 also results in the largest discrepancy for the elevator setting in trimmed conditions, where ROMv1 and ROMv2 are trimmed at much closer elevator deflection values.

Then, the aerodynamic forces and pitching moment produced with the trimmed HFM control inputs are compared at landing and cruise conditions. Tables 7 and 8 show the results of the comparisons at these two conditions,

respectively. In addition to the absolute values of lift, drag, and aerodynamic pitching moment, the relative error produced by each ROM is also shown as a heatmap. Cells in green indicate the smallest error produced between the three ROMs, while red indicates the largest.

Table 6: Angle of attack and control inputs of different ROMs in trimmed landing conditions (h = 5 m, $V_a = 50 \text{ m/s}$, $\delta_{\text{flap}} = 5 \text{ deg}$, DEP on)

ROM Version	α (deg)	$\delta_{ m elev}$ (deg)	DEP (0-1)	HTU (0-1)
HFM	5.3992	-8.3459	0.4453	0.0300
ROM v1	5.9123	-8.6563	0.4263	0.0580
ROM v2	5.8320	-8.5535	0.4084	0.0754
ROM v3	5.1971	-7.6390	0.4065	0.0598

Table 7: Lift, drag, and aerodynamic pitching moments produced by different ROMs at landing conditions (h = 5 m, $V_a = 50 \text{ m/s}$, $\delta_{\text{flap}} = 5 \text{ deg}$, DEP on)

ROM Version	L (N)	D (N)	My,ae (N m)
HFM	69 147.1	4 572.0	3 269.1
ROM v1	66 755.7	4 494.5	4 422.1
ROM v2	67 000.2	4 520.6	4 310.4
ROM v3	70 139.6	4 571.9	4 310.4
		Error (%)	
ROM v1	-3.5%	-1.7%	+35.3%
ROM v2	-3.1%	-1.1%	+31.9%
ROM v3	+1.4%	-0.0%	+31.9%

Table 8: Lift, drag, and aerodynamic pitching moments produced by different ROMs at cruise conditions (h = 1219 m, $V_a = 72.7 \text{ m/s}$, $\delta_{\text{flap}} = 0 \text{ deg}$, DEP off)

ROM	L D		My,ae
Version	(N)	(N)	(N m)
HFM	69 101.1	5 344.6	0.0
ROM v1	69 231.3	5 423.8	-860.6
ROM v2	73 849.1	5 473.6	-4 203.5
ROM v3	91 809.3	6 234.8	-4 549.5
	Erro	r (%)	Error (N m)
ROM v1	+0.2%	+1.5%	-860.6
ROM v2	+6.9%	+2.4%	-4 203.5
ROM v3	+32.9%	+16.7%	-4 549.5

While all ROM versions are able to produce reasonably similar values as the HFM, the simplest ROMv3 most closely replicates the lift and drag forces at the landing condition. On the other hand, the pitching moment shows a larger relative discrepancy between the HFM and ROMs, where ROMv2 and ROMv3 produce the closest value. The pitching moments produced by ROMv2 and ROMv3 are identical, as the only additional dependency included for the pitching moment coefficient lookup table in ROMv2 is the flap deflection, as compared to ROMv3. While ROMv3 produces the most accurate results at landing conditions, the opposite is true at cruise conditions, where ROMv1 produces significantly more accurate values. This is most apparent when observing the values of the aerodynamic pitching moment. While the DEP is deactivated at cruise conditions, ROMv2 and ROMv3 are produced with a fixed 0.5 DEP activity factor setting. This means that these two versions always assume the presence of a blown-wing effect, leading to large discrepancies in conditions where the DEP is not used (or used at a different setting). Additionally, the lack of dependency on the flap deflection further reduces the accuracy of ROMv3, which is produced with a fixed flap deflection of 5 deg. These results show that while simplified ROMs may indeed represent the aircraft dynamics accurately at some conditions, they come at the cost of reduced accuracy at other conditions that are farther from the ROM's evaluation point.

A further comparison was made by simulating the HFM and ROMs with the same constant control inputs from the same initial condition (again, trim inputs for the HFM at cruise condition) for 1000 seconds. This open-loop simulation was done without any controllers, therefore the response produced is purely due to the aero-propulsive model. The results of the simulation are shown in Figure 6. The first observation to be made is that the HFM is able to stay at roughly constant conditions, meaning that the aircraft is indeed trimmed. ROMv1 and ROMv2, while producing similar responses, differ in several ways. As they produce slightly different aerodynamic forces and pitching moments under the same conditions, the trim inputs for the ROM versions are not equal to those of the HFM, nor are they equal to each other. As a result, with the same inputs the different ROM versions settle at slightly different conditions. Both ROMv1 and ROMv2 settle at constant angles of attack that are lower than the HFM. In terms of airspeed, ROMv1 produces a response with a constantly decreasing airspeed, albeit at a very shallow slope, while the opposite is true for ROMv2. This results in a constantly decreasing altitude for ROMv1, while the simulation for ROMv2 shows an increase in altitude. On the other hand, the response produced by ROMv3 shows the loss of dynamic

stability altogether, as the aircraft fails to settle at a constant condition while the amplitude of the oscillations in all states (apart from horizontal distance) continues to grow throughout the simulation.

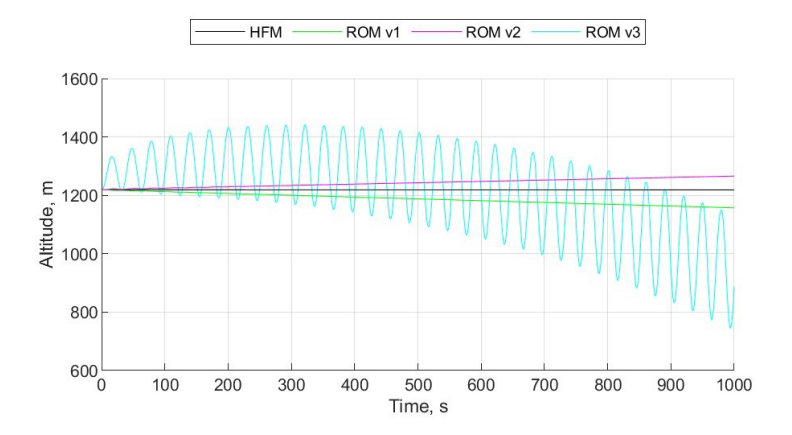


Figure 6: Open-loop simulation results, ROM v1-v3

On the basis of the three comparisons discussed above, a few conclusions can be made. The fidelity of a ROM in terms of the number of aerodynamic dependencies taken into account determines how closely it can mimic the magnitudes of the lift, drag, and pitching moment produced by the HFM at the same flight conditions. Discrepancies in lift, drag, and pitching moment will then manifest in the aircraft's physical behavior by altering its dynamic response. This is apparent in two ways when observing the aircraft's open-loop response. First, the four models exhibit dissimilar equilibrium points. Naturally, this also implies that their trim solutions are not interchangeable. Second, differences in the aircraft's dynamic stability are apparent. In the case of ROMv3, complete loss of dynamic stability is clearly indicated by diverging oscillations on all state variables. While this is a clear indication of reduced modeling accuracy, it should be noted that it would not necessarily create an issue in path performance optimization. As unstable flight should not contribute positively toward minimizing any well-defined cost function, the optimal control solver would naturally be incentivized to find solutions that avoid this behavior, effectively resulting in stability augmentation.

4.2 Path Performance Optimization

Optimal path performance is then evaluated using the three ROMs with the same objective functions, bounds, and constraints as outlined in Section 3.3. Throughout the trajectory optimization, the convergence of ICLOCS was highly sensitive to the bounds and constraints that were imposed, as well as to the numerical settings required by the IPOPT convergence tolerance. The latter has been tuned through a trial-and-error approach. The resulting state and control trajectories are shown in Figures 7 and 8 respectively. Table 9 shows top-level performance of all three optimizations.

Metric	ROMv1	ROMv2	ROMv3
Final time, s	1745.4	1064.2	684.2
Final distance, km	103.3	65.4	47.0
Avg. glide slope, deg	-0.67	-1.06	-1.48
Computation time, s	83	21	54

Table 9: Summary of trajectory optimization results

Using ROMv3 to represent the aircraft aerodynamics model results in the best trajectory overall, terminating the landing approach at $t_f = 684.2s$. ROMv1 and ROMv2 result in considerably longer landing times. In particular, ROMv3 produces a minimum time that is more than 60% lower than ROMv1. This is also reflected by the differences in the horizontal distance at which the aircraft reaches the prescribed terminal altitude as well as the average glide slopes achieved between the three ROM versions.

DEP and HTU usage for all three solutions present similar overall trends, where the DEP is set much higher than the HTU, which is used to produce negative thrust at the early and late stages of the trajectory. For all solutions, it is seen that the solver struggles to produce a smooth transition between the approach and terminal condition, as can be seen by the sharp drop in airspeed in the final parts of the trajectory in order to satisfy the boundary condition. The pitch angle bounds were also observed to be a limiting value. As the aircraft approaches the terminal altitude, a

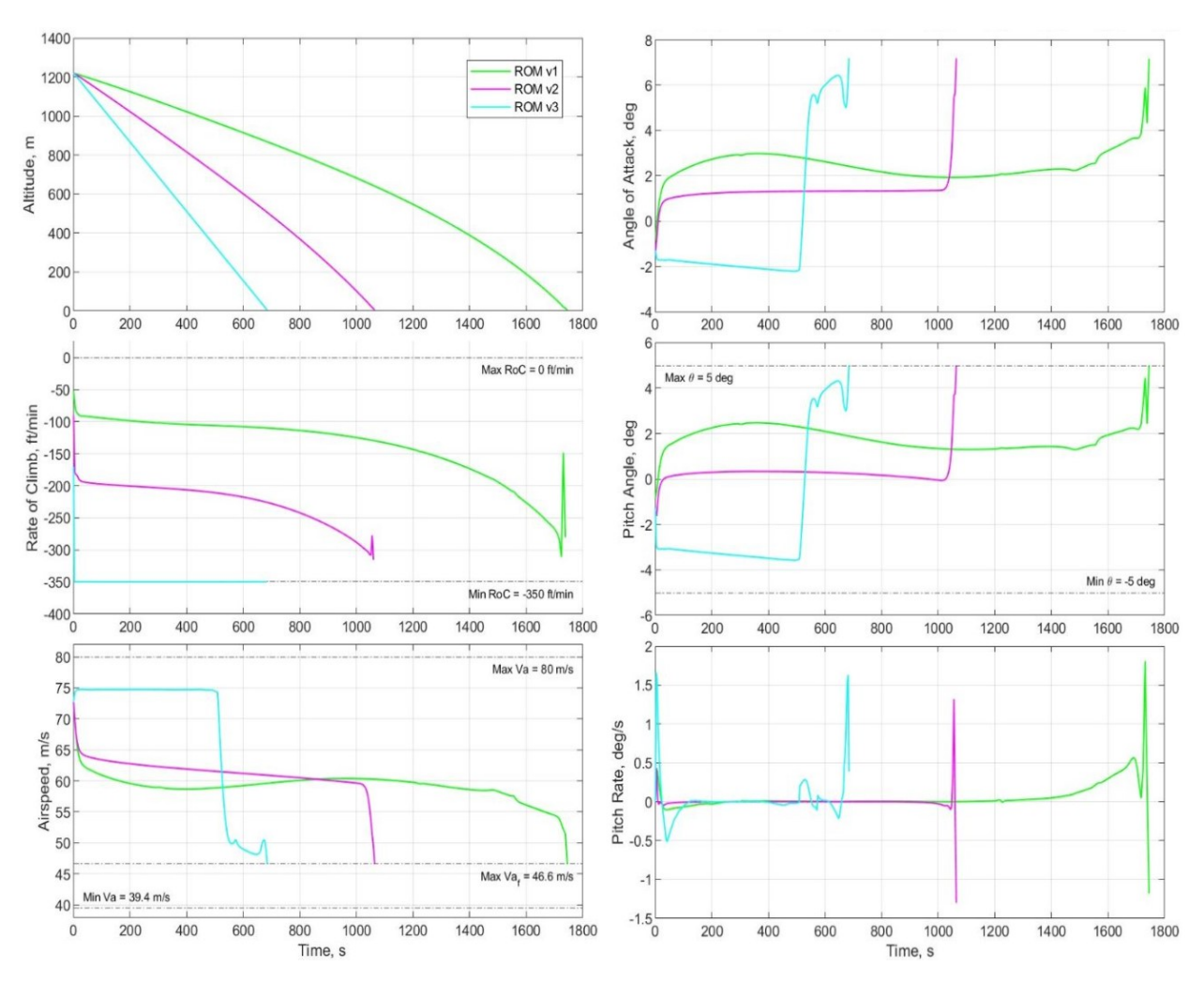


Figure 7: Optimal trajectories produced with all ROM versions, state variables

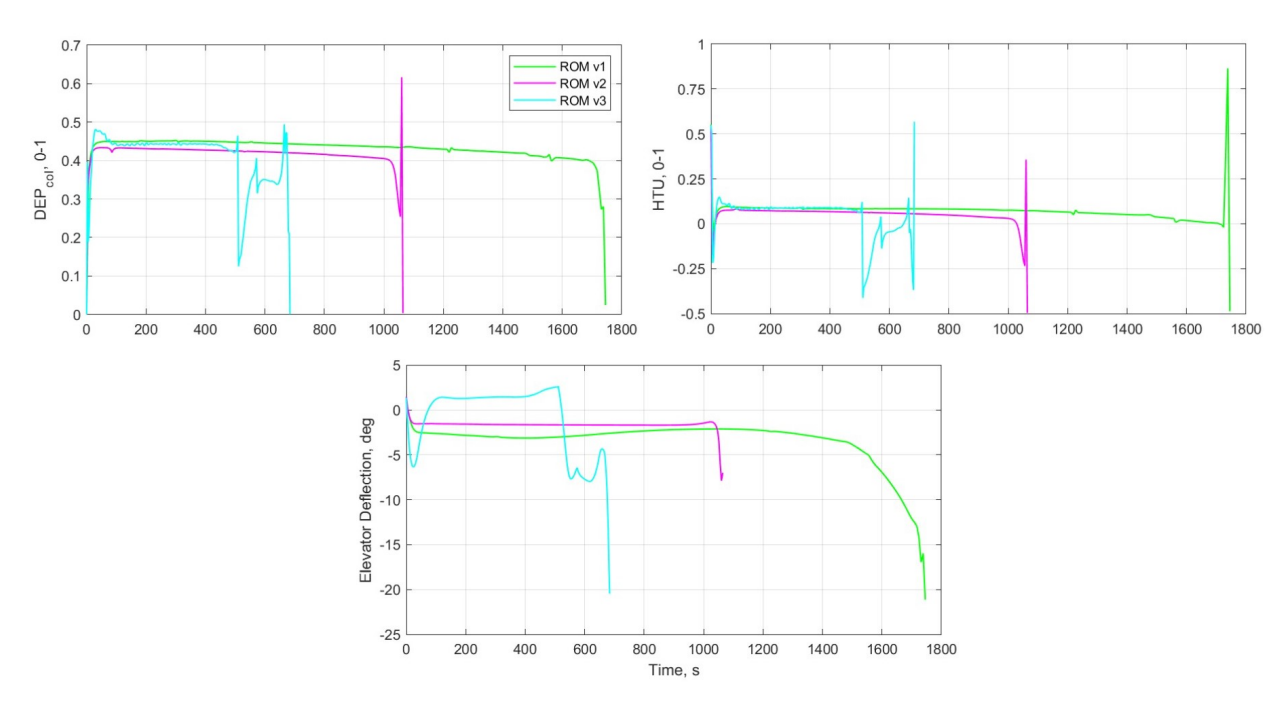


Figure 8: Optimal trajectories produced with all ROM versions, control variables

Table 10: Mean tracking error for all three ROMs

	Avg. LSED, m
ROMv1	0.4653
ROMv2	0.5218
ROMv3	0.5688

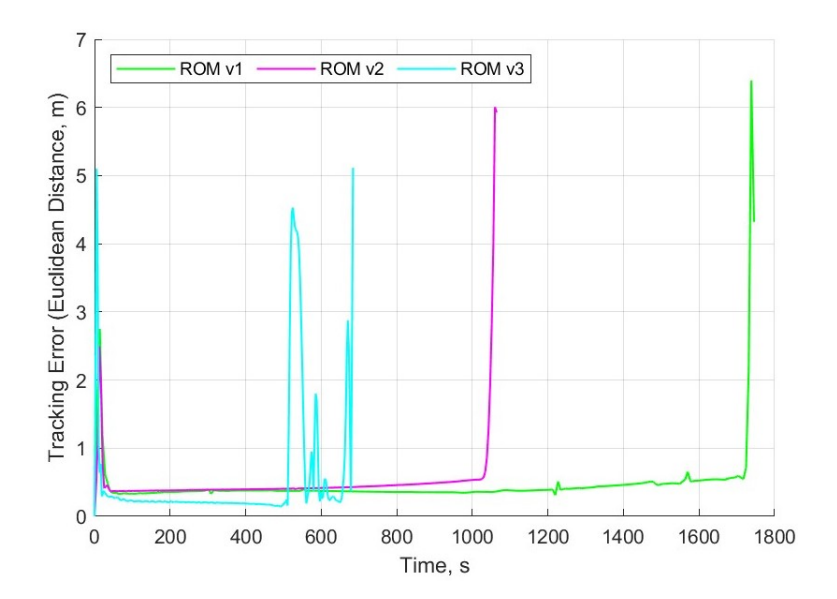


Figure 9: Tracking error comparison for all three ROMs

sharp flare maneuver is seen by deflecting the elevator which causes the aircraft to pitch up to the maximum allowable pitch angle. This maximum pitch angle was chosen to limit the aircraft to a reasonable attitude and maintain passenger comfort, preventing the solver from using excessively high pitch angles.

4.3 Tracking

The three optimal trajectories presented above were tracked using the HFM equipped with the altitude and airspeed control systems outlined in Section 3.4. The tracking error, represented by the Euclidean distance in the summation term of Equation 3, is plotted for all three trajectories as a function of time and shown in Figure 9. The average LSED, as defined by Equation 3, is shown in Table 10 for each one of the three ROMs.

While the HFM manages to track the references closely throughout a majority of the approach, sharp changes towards the start and end of the trajectories result in steep jumps in tracking error. This is an indication that the optimal trajectories resort to unrealistic maneuvers, particularly at the end of the approach, as the solver tries to satisfy the imposed terminal conditions.

The full-order model was able to closely track all trajectories by an average tracking error of under 60 cm. As expected, there is an increase in tracking error as the number of aerodynamic dependencies is reduced in the ROM used when producing the optimal trajectories. In particular, the optimal trajectory produced using ROMv1 was tracked with an 18% smaller average tracking error compared to ROMv3. This shows that while it is indeed true that including more aerodynamic dependencies allows for the calculation of more flyable optimal trajectories, the differences in terms of tracking error are modest, and even the simplest ROM was still able to produce a reasonably realistic result.

5. Conclusions and Recommendations

The terminal approach trajectories for the UNIFIER C7A have been evaluated for a minimum time objective supplemented by a stage cost function to penalize high airspeeds at low altitudes.

Three different ROMs with varying levels of fidelity with respect to the number of aerodynamic dependencies accounted for were used, resulting in significantly different results in terms of the time needed for the aircraft to reach the terminal landing conditions from cruise conditions. The simplest ROM version with the fewest aerodynamic dependencies resulted in the shortest approach trajectory while increasing aerodynamic dependencies (and therefore increasing model accuracy) also increased the time needed for the aircraft to complete the landing approach. While there are variations in computation time, all three solutions were generally produced quickly, with the longest calculation only taking 83 seconds.

When the resulting optimal trajectories were tracked using the HFM equipped with a PID tracking control system, it was observed that the trajectories produced with more accurate ROMs were tracked more closely. With that being said, all three resulting trajectories were still successfully tracked closely, with a mean tracking error (represented by

the average LSED) of under 60 cm for all ROM versions. The differences in trackability of the three solutions can therefore be considered marginal.

It should be noted that only a relatively simple tracking control system is used for this study. In reality, a more advanced automatic flight control system may be implemented with better tracking performance. This means that the trackability of the trajectories measured can be considered conservative.

In conclusion, the simplest ROM with the fewest aerodynamic dependencies is the best option as it produces the best results (in terms of landing time minimization) by a considerable margin while still maintaining a reasonably realistic trajectory.

The disparity in optimal solutions demands further investigation on techniques to construct surrogate models for optimal path performance. Further research is also recommended in comparing the results with different objective functions. Additionally, as the tracking results are strongly dependent on the quality of the tracking control system, more advanced flight control system designs should also be explored. In particular, for the UNIFIER C7A, it would be beneficial to implement a more advanced throttle control system that can independently control the DEP and HTU, allowing for better utilization of the unique propulsion configuration. Applying this methodology to other aircraft models and flight scenarios is also recommended in order to verify its practicality for a wider range of applications.

References

- [1] D.E. Kirk. *Optimal Control Theory: An Introduction*. Dover Books on Electrical Engineering Series. Dover Publications, 2004.
- [2] Mariana Ratiu and Mariana Adriana Prichici. Industrial robot trajectory optimization- a review. *MATEC Web of Conferences*, 126:02005, 2017.
- [3] Abolfazl Shirazi, Josu Ceberio, and Jose A. Lozano. Spacecraft trajectory optimization: A review of models, objectives, approaches and solutions. *Progress in Aerospace Sciences*, 102:76–98, October 2018.
- [4] Runqi Chai, Kaiyuan Chen, Lingguo Cui, Senchun Chai, Gokhan Inalhan, and Antonios Tsourdos. *Advanced tra- jectory optimization, guidance and control strategies for aerospace vehicles: methods and applications.* Springer, Singapore, 2023.
- [5] Hongchu Yu, Alan T. Murray, Zhixiang Fang, Jingxian Liu, Guojun Peng, Mohammad Solgi, and Weilong Zhang. Ship Path Optimization That Accounts for Geographical Traffic Characteristics to Increase Maritime Port Safety. *IEEE Transactions on Intelligent Transportation Systems*, 23(6):5765–5776, June 2022.
- [6] Ahmed W.A. Hammad, David Rey, Amani Bu-Qammaz, Hanna Grzybowska, and Ali Akbarnezhad. Mathematical optimization in enhancing the sustainability of aircraft trajectory: A review. *International Journal of Sustainable Transportation*, 14(6):413–436, June 2020.
- [7] Harijono Djojodihardjo. Green Aircraft Technology Imperatives for Environmental Sustainability. *Applied Mechanics and Materials*, 815:273–281, November 2015.
- [8] Prasun N. Desai and Bruce A. Conway. Six-Degree-of-Freedom Trajectory Optimization Using a Two-Timescale Collocation Architecture. *Journal of Guidance, Control, and Dynamics*, 31(5):1308–1315, September 2008.
- [9] Robert D. Falck, Jeffrey Chin, Sydney L. Schnulo, Jonathan M. Burt, and Justin S. Gray. Trajectory Optimization of Electric Aircraft Subject to Subsystem Thermal Constraints. In 18th AIAA/ISSMO Multidisciplinary Analysis and Optimization Conference, Denver, Colorado, June 2017. American Institute of Aeronautics and Astronautics.
- [10] Fabrizio Oliviero and Kilian Swannet. Optimal Energy Management Strategies and Mission Profiles for a generic Hybrid Aircraft. In AIAA AVIATION 2023 Forum, San Diego, CA and Online, June 2023. American Institute of Aeronautics and Astronautics.
- [11] David Erzen, Lorenzo Trainelli, Carlo E. D. Riboldi, Alberto Rolando, Francesco Salucci, Fabrizio Oliviero, Jernej Pirnar, Thomas Koopman, Andres Znidar, Matej Andrejasic, Rok Lapuh, Johannes Soikkeli, and Gregor Cretnik. UNIFIER19: Final Concurrent Design Report, July 2021. unifier19.eu.
- [12] Jack P C Kleijnen and Robert G Sargent. A methodology for fitting and validating metamodels in simulation. *European Journal of Operational Research*, 2000.

- [13] D. Galbally, K. Fidkowski, K. Willcox, and O. Ghattas. Non-linear model reduction for uncertainty quantification in large-scale inverse problems. *International Journal for Numerical Methods in Engineering*, 81(12):1581–1608, 2010.
- [14] Carlo Bottasso, Alessandro Croce, and Domenico Leonello. Two-level model-based control of flexible multibody systems. November 2023.
- [15] S. Chen and S. A. Billings. Neural networks for nonlinear dynamic system modelling and identification. *International Journal of Control*, 56(2):319–346, August 1992.
- [16] Johannes Soikkeli, Drago Matko, and Thomas Koopman. UNIFIER19 Flight Dynamics Simulator Model Documentation, August 2022. https://github.com/soikkelij/unifier_fds.
- [17] Johannes S. Soikkeli, Drago Matko, and Thomas Koopman. Cascaded nonlinear dynamic inversion applied to a fixed-wing distributed electric propulsion aircraft. In *AIAA AVIATION 2023 Forum*. American Institute of Aeronautics and Astronautics, June 2023.
- [18] Mathworks. MATLAB 3DOF (Body Axes), 2023.
- [19] Agostino De Marco, Eugene Duke, and Jon Berndt. A general solution to the aircraft trim problem. In AIAA Modeling and Simulation Technologies Conference and Exhibit. American Institute of Aeronautics and Astronautics.
- [20] Mathworks. MATLAB Optimization Toolbox, 2014.
- [21] Imperial College London. ICLOCS2 Optimal Control Software. ee.ic.ac.uk/ICLOCS/default.htm.
- [22] Andreas Wächter and Lorenz T. Biegler. On the implementation of an interior-point filter line-search algorithm for large-scale nonlinear programming. *Mathematical Programming*, 106(1):25–57, March 2006. DOI 10.1007/s10107-004-0559-y.
- [23] E.J.J. Smeur and A Jamshidnejad. AE4301 Automatic Flight Control System Design Course Materials, 2023.
- [24] Yaguang Tao, Alan Both, Rodrigo I. Silveira, Kevin Buchin, Stef Sijben, Ross S. Purves, Patrick Laube, Dongliang Peng, Kevin Toohey, and Matt Duckham. A comparative analysis of trajectory similarity measures. GIScience & Remote Sensing, 58(5):643–669, July 2021.